Nwiabu, L. N.

Conductivity-Velocity Models for Optimum Hydrate Chemical Inhibitor Concentrations

lesi_puene@yahoo.com

Chemical/Petrochemical Engineering Department, Rivers State University,
Port Harcourt, Rivers State, Nigeria

This article is covered and protected by copyright law and all rights reserved exclusively by the Centre for Petroleum, Pollution Control and Corrosion Studies. (CEFPACS) Consulting Limited.
Electronic copies available to authorised users.

DOI: https://doi.org/10.37703
The link to this publication is https://ajoeer.org.ng/otn/ajoeer/2024/qtr-3/02.pdf

Conductivity-Velocity Models for Optimum Hydrate Chemical Inhibitor Concentrations Assessment

Nwiabu, L. N.[1]; Dagde, K. K.[2]; Akpa, J. G.[3]; Ehirim, E. O.[4]
[1,2,3,4]Chemical/Petrochemical Engineering Department, Rivers State University, Port Harcourt

*** Corresponding author email address**: lesi_puene@yahoo.com

ABSTRACT

Knowledge of the concentration of inhibitors in the flowline is necessary for operators to decide on how much more chemical inhibitors to inject to keep the flowline safe. A common flow assurance strategy of applying excessive dosages of an inhibitor to minimize the risk of pipeline blockage due to hydrate formation often results in more cost and severe impact on the environment. Current research interest is in chemical methods that require the optimum chemical dosage that will be just enough to keep the system safe from hydrate formation using knowledge of inhibitor concentrations in the flowline. One of the most efficient of the methods is the conductivity and velocity (C-V) technique. However, the method lacks mathematical models to interpret the correlation of variables in the experimental data. It also does not have a model that can be used as a predictor of new results. This work presents a second-degree regression predictive model equation as the formulation approach for mathematical models (MM) of electrical conductivity and velocity as a function of inhibitor concentrations, salt concentrations, and temperature, leveraging on the relationships of experimental parameters in the existing C-V method. Furthermore, an artificial neural network (ANN) model is developed and trained to predict inhibitor concentrations. To achieve all these, the study generated experimental data by carrying out series of laboratory works to determine salt and inhibitor concentrations in at varying temperatures using the conductivity-velocity (C-V) method. From the results, apart from the solution containing 30.0 wt% Mono Ethylene Glycol (MEG) and 5.0 wt% NaCl that has slightly larger deviations of – 0.7 and – 0.9 for MM and ANN respectively due to MEG inhibitor concentrations that were beyond the range of the training data, mathematical models and the ANN model generally agreed with experimental measurements in determining inhibitor concentrations.

Keywords: Hydrate, Flowline, Inhibitor

DOI: https://doi.org/10.37703
https://ajoeer.org.ng/otn/ajoeer/2024/qtr-3/02.pdf

INTRODUCTION

In mitigating and forestalling hydrate formation, chemical injection stands out as a widely employed strategy, lauded for its economic feasibility and technological viability (Linga et al., 2009). This approach entails the introduction of specialized additives into hydrocarbon pipelines to stave off the formation of gas hydrates during the conveyance of hydrocarbons.

These hydrate inhibitors can be categorized into two primary groups: thermodynamic hydrate inhibitors (THIs) and low-dosage hydrate inhibitors (LDHIs). Thermodynamic inhibitors, such as methanol (MeOH), monoethylene glycol (MEG), and ethanol, operate by shifting the hydrate phase boundary to lower temperatures and/or higher pressures through the reduction of water activity (Barker and Gomez (2000). This alteration allows the system to operate safely beyond the confines of the hydrate stability zone. In recent times, low-dosage hydrate inhibitors (LDHIs) have experienced rapid advancements (Argo et al., 2012; Fu et al., 2014). The LDHIs encompass kinetic hydrate inhibitors (KHIs) and anti-agglomerants (AAs).

Effectively overseeing and monitoring hydrate formation and inhibition is essential to ensure the routine and cost-effective operation of pipelines. Consequently, the management of hydrate formation through chemical means mandates precise chemical dosages that strike a harmonious balance between prevention and cost-efficiency. As underscored by a study conducted by Yan et al. (2014), both excessive and insufficient chemical dosages can yield adverse consequences, either inflating costs or exacerbating issues related to hydrate formation.

Currently, innovative techniques have emerged to assist operators in precisely determining the ideal dosage of chemical inhibitors for injection into flowlines. These methodologies offer accurate and timely data regarding the extent of hydrate inhibition within pipelines or processing facilities, essentially gauging how closely the operational conditions align with the Hydrate Stability Zone (HSZ). Among the methods is electrical conductivity measurement, and acoustic velocity (C-V) techniques. The C-V method is built on the widely acknowledged notion that the electrical conductivity of liquid solutions is contingent upon the concentration of ions and their activity. Typically, the aqueous fluids present in pipelines constitute electrolyte solutions, with conductivity being directly proportional to the salt concentration. The activity of these ions is influenced by factors such as temperature and the presence of nonconductive chemical additives. Measurements of electrical conductivity can effectively provide insights into the concentrations of various chemicals. Additionally, there is a correlation between sound velocity in seawater and parameters such as salinity and temperature (Clay and Medwin, 2017). Acoustic velocity has been used in several works to investigate solutions and binary gas mixtures (Goodenough et al., 2015; Vyas et al., 2006). The development of a methodology for ascertaining optimal hydrate chemical concentrations via the conductivity-velocity (C-V) technique hinges on the measurement of both electrical conductivity and acoustic velocity within an aqueous sample.

Although the application of the conductivity and velocity (C-V) technique for determining inhibitor concentrations in oil and gas flowlines to achieve optimal hydrate chemical injection

has proven highly effective and has entered commercial use, the technique lacks a standardized model for interpreting its experimental data. Furthermore, it lacks a model that can serve as a predictive tool for new results. This work employs a second-degree regression predictive equation to develop mathematical models (MM) of electrical conductivity and velocity as a function of inhibitor concentrations, salt concentrations, and temperature, leveraging on the relationships of experimental parameters in the existing C-V method. Laboratory experiments focused on the monitoring of hydrate chemical inhibition are conducted to generate data. These experiments utilized the existing conductivity-velocity method to investigate alterations in inhibitor concentrations and temperature, which impact both electrical conductivity and sound velocity. Furthermore, an artificial neural network (ANN) model is developed and trained with experimental data to predict inhibitor concentrations.

2. Related Works

In recent years a great deal of effort has been made to optimize hydrate inhibitor injection to minimize the cost and environmental impact. Willmon and Edwards (2016) suggested experience-based rules of thumb to help rationalizing the dosage of hydrate inhibitors. Lavallie et al (2022) proposed method consists in determining the parameters of the hydrate formation based on fixing the optical effect of the light source reflection distortion on the mirror-like "liquid-gas" interphase surface. This optical effect makes it possible to sensitively record the changes occurring at the micro level with a mirror-like interphase "gas-liquid" surface. This effect of the interphase boundary distortion is explained by the formation, growth, chaotic accumulation, and localization at this boundary of hydrate microcrystals of different shapes and sizes. A recent method of monitoring hydrate formation is the use of knowledge of existing concentrations of inhibitors in the flowline. The water activity method is one of the inhibitor concentration methods. A general correlation has been developed to relate the measured water activity values to the hydrate suppression temperate by generating pseudo, which is much easier than experimental data using a well-proven thermodynamic model (Avlonitis, 2014). Using pseudo-experimental data instead of real experimental data in developing the correlation makes it possible to generate a large database of different concentrations of salt and alcohol (methanol and MEG) solutions over a wide range of concentrations at a shorter time and lower cost. Despite the development of sophisticated hydrate phase equilibrium calculation models that are both the most accurate and most comprehensive, such as the vapour–solid equilibrium ratio (Ki value) method (Carson and Katz, 1942; Wilcox et al., 1941). The main advantage of

these techniques is the availability of input data and the simplicity of the calculation, which can be performed by using charts or hand-held calculators.

Since 1945, the gas gravity method given by Katz (1945) has been an indispensable and simple tool for predicting the gas hydrate stability zone. It only requires the specific gravity of the mixture, i.e., the molecular mass of the gas mixture divided by that of air. The original gas gravity method is only applicable to dry gas systems. However, the development of offshore/arctic oil and gas-condensate fields necessitated a robust and simple method for predicting the hydrate stability zone for these systems. Ostergaard et al. (2015) developed a method similar to the gas gravity method, applicable to all reservoir fluids, in the presence of distilled water, from natural gas to black oil, which only requires information on the specific gravity and the concentration of the hydrate forming components in the system. The method can take into account the effect of non-hydrocarbon gases (i.e., CO2 and N2) in the petroleum fluid. There also exist simple tools for estimating the hydrate inhibition effect of salts and organic inhibitors.

The most famous one is the Hammerschmidt (1934) equation, but also equations by Yousif and Young (1993) are available. These equations calculate the suppression of the hydrate dissociation temperature, ΔT, compared to that of distilled water (i.e., the hydrate phase boundary in the presence of distilled water should be determined separately). Inherently, they have the following simplifying assumptions, reducing their accuracy; ΔT is independent of the system pressure, ΔT is independent of gas/oil composition and hydrate structure. ΔT is independent of the inhibitor. Ostergaard et al. (2015) developed a correlation for predicting the hydrate stability zone of reservoir and drilling fluid in presence of thermodynamic inhibitors (i.e., electrolytes and organic inhibitors). This correlation requires inhibitor concentration, pressure of the system and if known the dissociation pressure of hydrocarbon fluid in the presence of distilled water at 273.12K. Mohammadi and Richon (2016) studied the possibility of estimating hydrate stability zone based on reflective index data of aqueous solution containing salt or organic inhibitor using an artificial neural network method. The correlation considers the changes in index of refraction with respect to refractive index of pure water for a given aqueous solution. In a very similar work, Mohammadi et al. (2016). have looked at the possibility of estimating hydrate stability zone from electrical conductivity data of salt aqueous solutions. This correlation cannot predict the effect of presence of thermodynamic inhibitor. Both of these correlations have been validated using only limited literature data. The centre for

Gas Hydrate Research at Heriot-Watt University developed a correlation based on freezing point depression which determines the hydrate safety zone (HSZ) by measuring the freezing point of the downstream water samples (Tohidi et al, 2009). A prototype developed for this method has its own limitation, particularly for high inhibitor concentration. To measure freezing point of an aqueous sample using the method, the sample need to be freezed. For high concentrations e.g., 50 mass% of MEG the system needs to be cooled to around -50oC to freeze the sample. The minimum temperature which the current prototype can reach is about -40 °C. The second limitation is that, in such high concentration limited amount of ice will form, hence accuracy is hindered. This method has also a limited potential for on-line application. Tohidi et al. (2008) had previously proposed a method for determining the stability margin of hydrate zone based on water content measurement in the gas phase. Similarly, Yang et al., 2011 developed the conductivity and velocity (C-V) method for two parameters systems (systems with two unknown salt and/or inhibitor concentrations), i.e., MeOH or MEG or KHI systems in the presence of salts. It was previously reported that the hydrate suppression temperature (i.e., dissociation temperature shift) of salt aqueous solution can be determined by measuring the electrical conductivity of an aqueous sample (Mohammadi, et al., 2016). Henning et al. (2017) developed an acoustic multi-sensor system for accurate measurements of concentrations of chemicals like MeOH and MEG. However, in most cases, there are salts and one inhibitor at least in the aqueous phase in a pipeline. To be able to determine both inhibitor and salt concentrations simultaneously two physical properties are at least to be known. Sandengen and Kaasa (2018) developed an empirical correlation that determined MEG concentration and NaCl concentration based on measurements of the density and electrical conductivity of water samples under examination. However, the requirement of high accuracy of the density measurement makes it hardly applicable to real produced water samples that usually contain solid particles (sands and clays) and oil droplets.

Bonyad et al (2021) developed a technique for optimizing hydrate inhibitor injection rates by monitoring the actual hydrate inhibitor concentrations downstream. The technique determines the salt and inhibitor concentrations by measuring speed of sound and electrical conductivity in an aqueous sample taken from pipeline/separator. Lavallie et al (2022) compared the automated laboratory C-V technique which combines the double measurements of water conductivity and ultrasonic sound velocity which are analysed by a method based on colorimetric titration which requires rather long manual analysis. Yang et al. (2023) developed a technique for measuring the concentration of salts, thermodynamic and kinetic hydrate

inhibitors in the aqueous phase based on integrated data collection on electrical conductivity and acoustic velocity of aqueous phase chemical composition. The work led to the determination of hydrocarbon fluid composition and, accordingly, hydrate stability zone recognition.

3. MATERIALS AND METHODS

This section presents the materials, equipment, and the methods used in carrying out the study. The methods entail the procedures used in laboratory experimental work, the formulation of a mathematical model to validate the experimental process, the development of an artificial neural network model using experimental AA, KHI, and thermodynamic systems data. Finally, the integration of the ANN model to a thermodynamic model to predict hydrate phase boundary.

3.1 Materials

The materials utilized in the experimental phase of this study encompass chemicals and equipment. The chemicals employed consist of (1) Deionized water (2) Thermodynamic inhibitors: ethanol and ethylene glycol (MEG) (3) Salts: NaCl (4) Kinetic Hydrate Inhibitors (KHI): commercial KHI and (5) Anti-agglomerants (AA): commercial water-soluble AA and oil-soluble AA. The equipment comprises (1) Electrical Conductivity Meter (2) Ultrasound Pulse Generator (3) Ultrasound Transducer (4) Data Acquisition Board and (5) Measurement Cell.

3.2 Methods

The methods involve the procedures used in laboratory experimental work, the formulation of a mathematical model to validate the experimental process, the development of an artificial neural network model using experimental data. Then, the assessment of HSZ of a thermodynamic system using inhibitor and salt concentrations determined by the ANN model.

3.2.1 Experimental Setup

A microcontroller-based wave generator with an integrated 16-bit AD converter was employed to measure the induced voltage, which was then translated into electrical conductivity (Figure 3.1). Additionally, temperature was monitored using an 8-bit AD converter that was part of the system. The collected data was transmitted to a computer through an RS232 serial port.

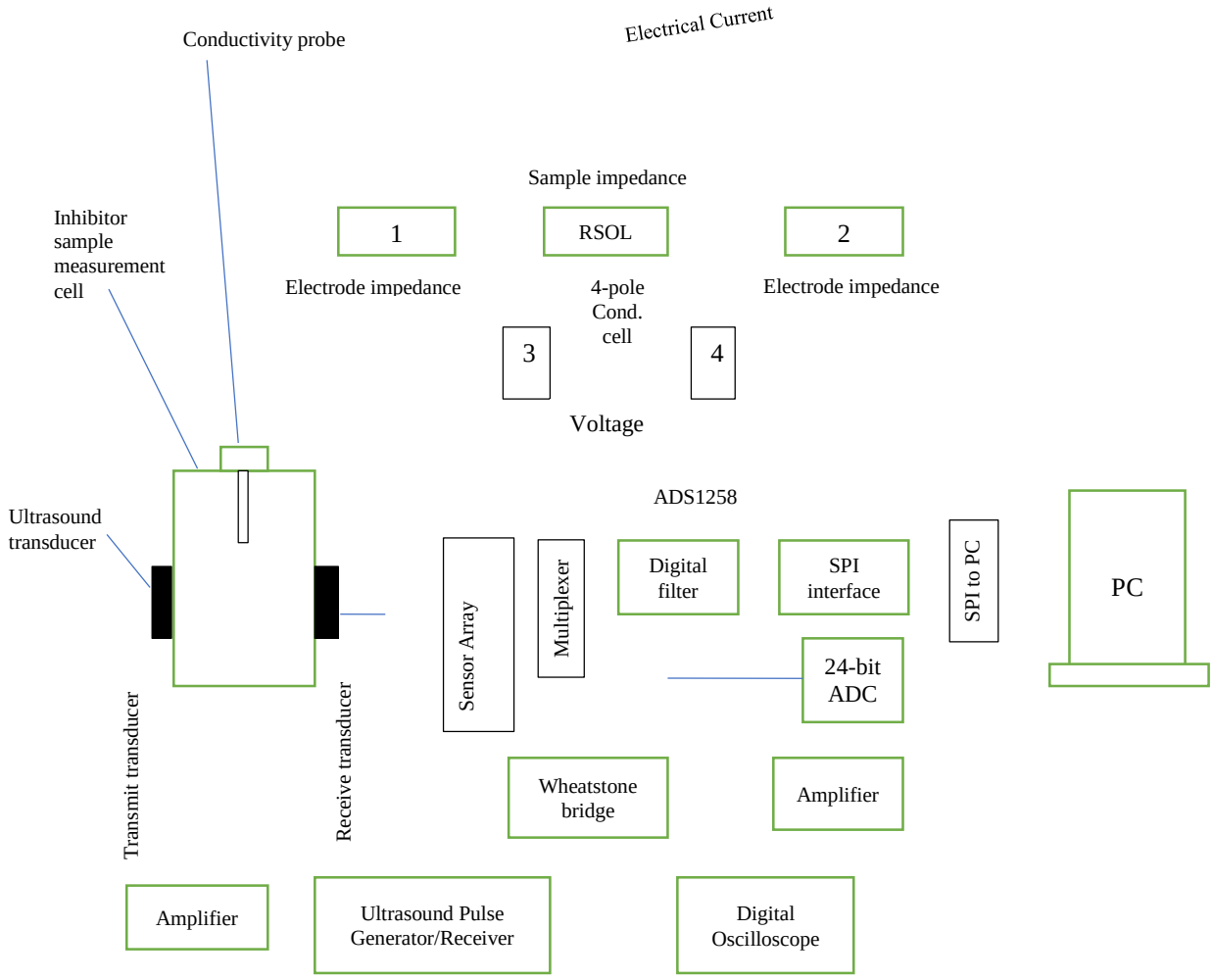

Figure 3.1: Schematic diagram of the experimental setup

To measure sound velocity, a pair of Panametric V104 ultrasound transducers operating at a frequency of 1 MHz was employed. These transducers were responsible for both transmitting the sound wave and receiving data as it passed through the sample within the cell. A standard ultrasound pulse generator (PR5072) was utilized to produce a pulse of -100 volts, which effectively excited the ultrasound transducer. The pulse generator was configured to operate at 1 MHz to align with the specifications of the ultrasound transducers.

For capturing the ultrasound wave, a high-frequency data acquisition board was utilized. This board featured an ultrafast 8-bit Atmel ADC and a Xilinx Spartan FPGA (Field Programmable Gate Array). The substantial volume of raw data collected was then transferred to the computer via a Universal Serial Bus (USB 2.0) connection.

3.2.2: Experimental Procedure

A process was initiated where approximately 120 ml of prepared aqueous solutions were introduced into the C-V cell. To maintain precise control over the measurement temperature, a thermostat connected to a cooling jacket that enveloped the sample cell was employed. Measurements of both conductivity and velocity were performed at various temperatures, including 0, 4, 15, and 25 ºC for the two-parameter measurement method, and at 10 and 20 ºC for the three-parameter method. To ensure accurate results, each test sample was held at its designated temperature for a minimum of one hour to achieve thermal equilibrium. All measurements were carried out under atmospheric pressure.

To guarantee measurement accuracy, the conductivity meter underwent calibration using a 0.1D KCl standard solution, while the velocity measurement was calibrated using deionized water.

3.2.3: Data Collection and Analysis

The data collected from multiple experimental runs were gathered and subjected to analysis. This analysis aimed to uncover patterns, acquire knowledge, and unveil relationships among the various data variables. This information was leveraged for two primary purposes: (1) the development of a mathematical model to validate the C-V technique, and (2) the training of an artificial neural network (ANN) model capable of predicting salt and inhibitor concentrations based on conductivity and velocity measurements at different temperatures.

3.2.4: Pre-Processing of experimental data

The data came with noise, gaps, and inconsistencies that made it unsuitable for direct use in algorithms without some preprocessing. To enhance prediction accuracy, a preprocessing step is applied to the experimental data. This preprocessing includes normalization, data balancing, and cropping. To ensure consistency in the ANN model, the data is divided into segments, each with a fixed length, and then normalized using z-score normalization.

The convergence of a neural network works better when the data follows a normal distribution. Equation (3.1) is employed for normalization:

$$\text{Normalization (X)} = \frac{x - \bar{x}}{s} \quad (3.1)$$

Here, 'x' represents the data value, '$\overline{x}$' is the average, and 's' is the standard deviation.

The issue of data balance or class imbalance is also addressed because the distribution of datasets can impact training outcomes. Imbalanced datasets can lead to the over-detection of certain classes in the output, particularly those with more data. To tackle dataset imbalance, a specific percentage of the majority class was adopted.

3.2.5: Formulation of Mathematical Models

From the experiment, electrical conductivity is a function of salt concentration, inhibitor concentration and the operating temperature. The models incorporated inhibitor concentration, salt concentration, and temperature as independent variables and electrical conductivity as the dependent variable to validate the C-V technique. To achieve this, the study employs a second-degree regression predictive model equation as the formulation approach.

Electrical Conductivity (EC) Model

$$\text{EC} = f(C_s, C_i, T)$$

$$EC = \beta_O + \beta_1 C_s + \beta_2 C_i + \beta_3 T + \beta_{12} C_s C_i + \beta_{13} C_s \text{T} + \beta_{23} C_i \text{T} + \beta_{11} {C_s}^2 + \beta_{22} {C_i}^2 + \beta_{33} T^2 + \text{e}i \quad 3.2$$

The errors in EC are obtained by rewriting equation (3.13) as:

$$ei = EC - \beta_o - \beta_1 C_s - \beta_2 C_i - \beta_3 T - \beta_{12} C_s C_i - \beta_{13} C_s T - \beta_{23} C_i T - \beta_{11} {C_s}^2 - \beta_{22} {C_i}^2 - \beta_{33} T^2 \quad 3.3$$

$$e_i^2 = \left(EC - \beta_0 - \beta_1 C_s - \beta_2 C_i - \beta_3 T - \beta_{12} C_s C_i - \beta_{13} C_s T - \beta_{23} C_i T - \beta_{22} {C_i}^2 - \beta_{33} T^2\right)^2 \quad 3.4$$

The sum of the squares of these errors is written as:

$$\sum_{i=1}^{n} e_i^2 = \left(EC - \beta_0 - \beta_1 C_s - \beta_2 C_i - \beta_3 T - \beta_{12} C_s C_i - \beta_{13} C_s T - \beta_{23} C_i T - \beta_{11} {C_s}^2 - \beta_{22} {C_i}^2 - \beta_{33} T^2\right)^2 \quad 3.5$$

$$let\ L = \sum_{i=1}^{n} e_i^2\ and\ subjecting\ partial\ derivative\ {}^{\partial_L}/_{\partial\beta_0} = Zero \quad 3.6$$

$$\frac{\partial l}{\partial_{\beta_0}} = -2 \sum_{i=1}^{n} \left(EC - \beta_0 - \beta_1 C_s - \beta_2 C_i - \beta_3 T - \beta_{12} C_s C_i - \beta_{13} C_s T - \beta_{23} C_i T - \beta_{11} {C_s}^2 - \beta_{22} {C_i}^2 - \beta_{33} T^2\right) = 0 \quad 3.7$$

Similarly, the **Velocity (V) Model** was developed as:

$$\text{V} = f(C_s, C_i, T)$$

$$V = \beta_O + \beta_1 C_s + \beta_2 C_i + \beta_3 T + \beta_{12} C_s C_i + \beta_{13} C_s \text{T} + \beta_{23} C_i \text{T} + \beta_{11} {C_s}^2 + \beta_{22} {C_i}^2 + \beta_{33} \text{T} + \text{e}i \quad 3.8$$

EC and V represent electrical conductivity and sound velocity respectively, which are the variables predicted. Cs, Ci, and T stand for salt concentrations, inhibitor concentrations, and temperature, respectively, serving as the independent or predictive variables. The term "ei" represents the error terms, accounting for the model's inability to precisely match the data. L represents the sum of the squared error terms. β0, β1, β2, and β3 are the regression coefficients of the model, which are constant values estimated from the data. β0 is the constant intercept, representing the V value when Cs = 0, Ci = 0, and T = 0. β1 is the partial regression coefficient indicating the contribution of salt concentrations (Cs) to electrical conductivity (EC) and sound velocity (V), adjusted for inhibitor concentrations (Ci) and temperature (T). β2 represents the partial regression coefficient indicating the impact of inhibitor concentrations (Ci) on sound velocity (V), adjusted for salt concentrations (Cs) and temperature (T). Similarly, β3 is the partial regression coefficient showing the influence of temperature (T) on sound velocity (V), adjusted for salt concentrations (Cs) and inhibitor concentrations (Ci). The notations β11c_s^2, β22c_i^2, β33T^2 represent the squared effects of salt concentrations, inhibitor concentrations, and temperature, respectively. On the other hand, β12c_s c_i, β13c_s T, β23c_i T represent the interactions between salt concentrations and inhibitor concentrations, salt concentrations and temperature, and inhibitor concentrations and temperature, respectively.

3.2.6: Artificial Neural Network Model

An artificial neural network (ANN) model was developed and trained with the generated laboratory experimental data. An artificial neural network comprises numerous computational units known as neurons, interconnected by weighted communication links, as illustrated in Figure 3.2.

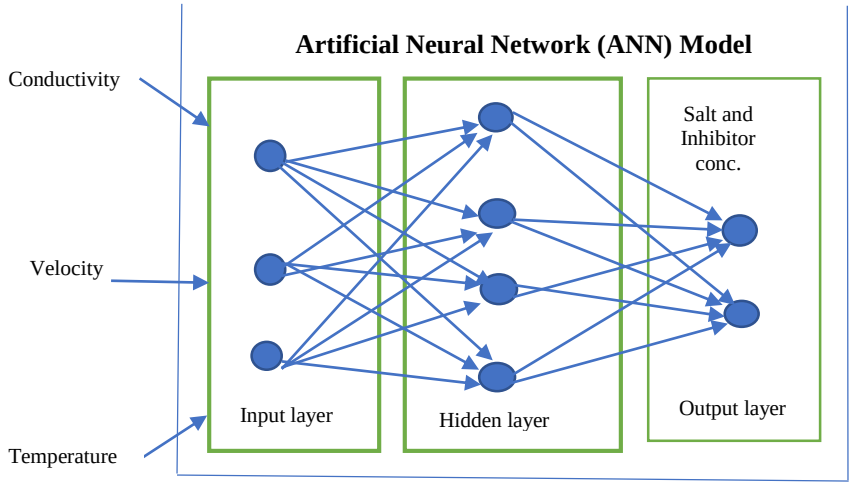

Figure 3.2: ANN Model for determining salt and inhibitor concentrations

The input layer of the network is responsible for receiving all input data and presenting scaled data to the network. Information from the input neurons is transmitted through the network via these weighted connections. Each neuron in a given layer, denoted as the "k" layer, is linked to every neuron in adjacent layers. Within the hidden "k" layer, each neuron performs the following tasks: it computes the sum of the incoming weighted inputs (input vector Ii = [I1, I2, ..., INk-I]) and then transmits this summation through a non-linear activation function, denoted as "f," to the adjacent neurons in the next hidden layer or to the output neuron(s). In this particular study, the activation function employed is a sigmoid function:

$$f(x) = \frac{1}{1+e^{-x}} \qquad x \in [0,1] \tag{3.9}$$

A bias term, *b*, is associated with each interconnection in order to introduce a supplementary degree of freedom. The expression of the weighted sum, *S*. to the i^{th} neuron in the k^{th} layer ($k \geq 2$) is:

$$S_{k,i} = \sum_{j=I}^{N_{K-I}} \left[\left(w_{k-1,j,i} I_{k-1,j} \right) + b_{k,i} \right] \tag{3.10}$$

Where *w* is the weight parameter between each neuron-neuron interconnection. Using this simple feed-forward networks with non-linear sigmoid activation functions, the output, 0, of the i neuron within the hidden *k* layer is therefore:

$$O_{k,i} = \frac{1}{1+e^{-\left(\sum_{j=1}^{N_{k-1}} \left[\left(w_{k-1,j,i}\, I_{k-i,j} \right) + b_{k,i} \right] \right)}} = \frac{1}{1+e^{-S_{k,i}}} \tag{3.11}$$

For the use with the neural network, the input data, *X*, were normalized and centred:

$$X_i^{\,I} = 0.1 + 0.8 \frac{X_i^{\,I} - X_{i,min}}{X_{i,max} - X_{i,min}} \tag{3.12}$$

Where X*i* is the i^{th} values of the input data fed to the input neuron *i*, and $X_{i,min}$ is the minimal value of the input data fed to the same *i* neuron and inversely $X_{i,max}$ is the maximal value. To achieve a better stability and to have output of the same order of magnitude, the following scaling rule was applied to salt and inhibitor concentrations before normalisation:

$$X_{Network} = In\left(X_{exp}\right) \tag{3.13}$$

In the case of the ethanol-salt system, the data was segregated into two groups: the first group encompassed ethanol concentrations ranging from 0 to 20 wt%, and the second group covered

concentrations from 30 to 50 wt%. In both scenarios, the NaCl concentration ranged from 0 to 10 wt%. Based on this data analysis, two separate ANNs were trained to predict ethanol and salt concentrations. The network structure for training was similar to the AA-Salt models, with slight adjustments such as a reduced number of inputs (two) due to a constant temperature (20 °C) and a smaller set of data, resulting in a hidden layer with 5 neurons.

In the KHI and salt system, we employed a design with 2 inputs (conductivity and velocity) and two outputs for the ANN. We opted for five neurons in the hidden layer due to the observed sensitivity of sound velocity and electrical conductivity to changes in KHI and salt concentrations.

For the MEG-KHI-NaCl system, we prepared two sets of data for ANN development. In both datasets, we utilized conductivity and velocity at 25 °C as two of the three required parameters. In the first set, we included the conductivity thermal coefficient as the third parameter, while in the second set, we used the sound velocity thermal coefficient to determine which coefficient would yield better ANN prediction performance. To train the ANN, we defined a network structure with 3 inputs and 3 outputs. After several trials, we settled on using 7 neurons in the hidden layer.

ANN Training

During the training process, input variables are supplied to the network, and the difference between the experimental outputs and the calculated outputs serves as the criterion for adjusting the network's synaptic weights. Initially, all synaptic weights and biases are randomly initialized. The network undergoes training, and its synaptic weights are fine-tuned using an optimization algorithm until it accurately replicates the input/output mapping by minimizing the average root mean square error. This work employed the Levenberg-Marquardt algorithm (Levenberg, 1944; Marquardt, 1963) as the chosen optimization method. The Levenberg-Marquardt optimization algorithm involves modeling the network's synaptic weights using the following formula:

$$w_j = w_{j-i} - \left[\bar{H}(w_{j-i}) + \mu_j \bar{I}_d\right]^{-1} \nabla J(w_{j-1}) \quad 3.14$$

With

$$\bar{H}(w_j) = \sum_{k-I}^{N} \left(\frac{\partial err^k}{\partial w_j}\right)\left(\frac{\partial err^k}{\partial w_j}\right)^T + \sum_{k=I}^{N} \left(\frac{\partial^2 err^k}{\partial w_j \partial w_j{}^T}\, err^k\right) \quad 3.15$$

Where err^k, μ, J, N are the residue vector, the step values of the Levenberg-Marquardt method Equation 3.63 and Equation 3.64, the Jacobian matrix of the first derivative of global error to weight and the number of feed inputs, respectively. ∂err^k is defined by:

$$err^I = Y^I{}_{exp.} - Y_{cal}{}^I \quad 3.16$$

Finally, inhibitor and salt concentrations are then re-transformed to their original scale.

4. RESULT AND DISCUSSION

The electrical conductivity and velocity experiments encompassed all three categories of hydrate inhibitors: thermodynamic hydrate inhibitors, KHIs, and AAs, under varying conditions, including the presence and absence of salt. Specifically, we investigated thermodynamic inhibitors like methanol and ethylene glycol, KHIs, and AAs. Additionally, we measured the mathematical model and the ANN model results to validate the C-V method's experimental data. The outcomes of the models closely align with the experimental data. From Figures 4.1, 4.2, and 4.3, it's evident that at every data point, the ANN predictions are closer to the experimental values compared to the predictions from the mathematical model (MM). While there are some cases of overlap where both models agree with the experimental data (true values), overall, the graphs demonstrate that the predicted concentrations by the ANN align more closely with the experimental values in comparison to the MM's predictions. This suggests that the ANN model is performing better in capturing the underlying relationships in the data and providing more accurate predictions.

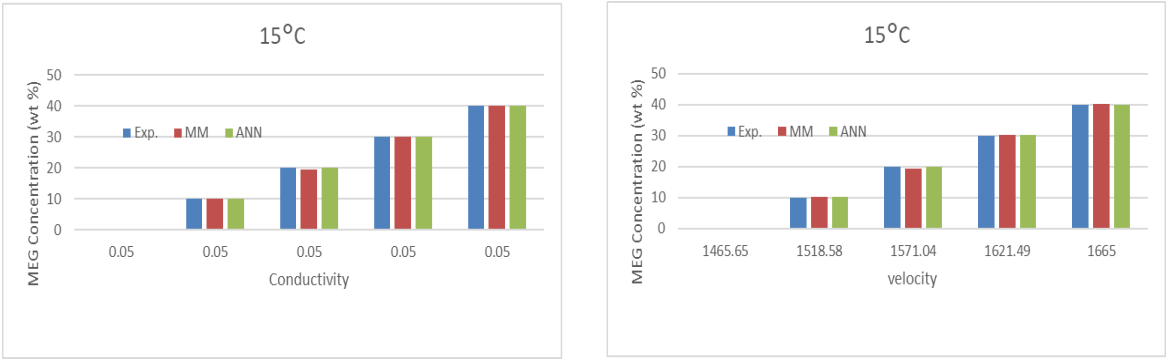

Fig 4.1: EXP, MM, and ANN results on the effect of conductivity and velocity on **MEG** concentrations at 15°C

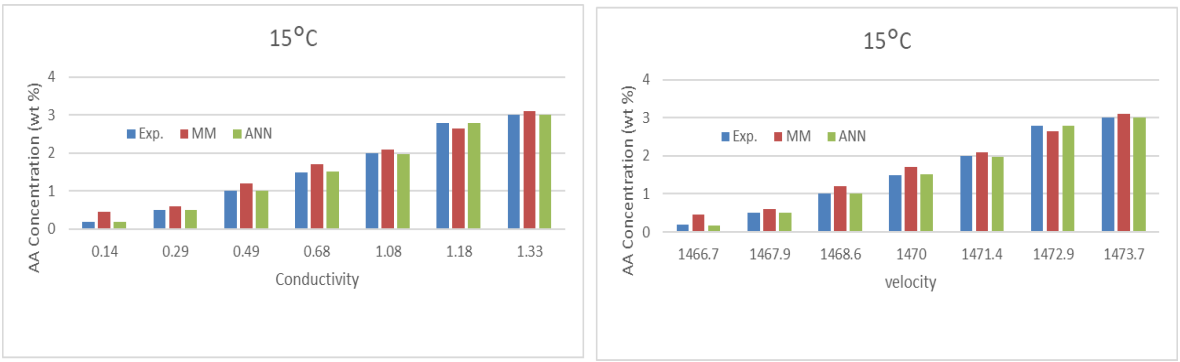

Fig 4.2: EXP, MM, and ANN results on the effect of conductivity and velocity on **AA** concentrations at 15°C

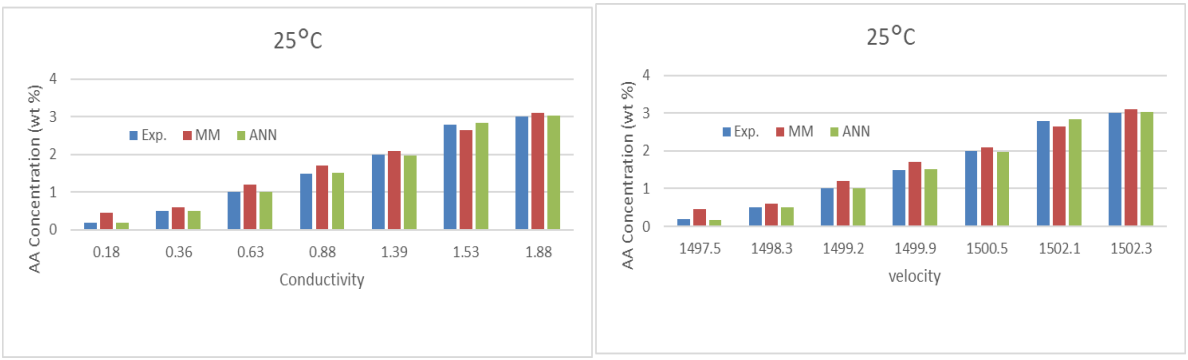

Fig 4.3: EXP, MM, and ANN results on the effect of conductivity and velocity on **AA** concentrations at 25°C

To evaluate the inhibitor systems, results of the mathematical models and results of the ANN model were compared with experimental data. Table 4.1 contains a sample of specific predictions evaluated.

Table 4.1: Evaluation results of MM and ANN models, in wt%

		PARAMETERS			**RESULTS**				
Inhibition systems	**Hydrate Inhibitors**	**Temp (°C)**	**Conductivity (ms/cm)**	**Velocity (m/s)**	**Concentrations**			**AD**	
					EXP	MM	ANN	MM	ANN
AA-NACL	AA	4	10.65	1438.9	1.50	1.60	1.45	0.10	- 0.05
	NACL	4	10.65	1438.9	1.00	1.24	0.99	0.24	- 0.01
AA-NACL	AA	4	29.57	1460.9	0.20	0.20	0.20	0.0	0.0
	NACL	4	29.57	1460.9	3.00	3.10	2.97	0.10	- 0.03
AA-NACL	AA	15	14.28	1482.7	2.00	2.10	2.10	0.10	0.10
	NACL	15	14.28	1482.7	1.00	1.16	1.00	0.16	0.0
AA-NACL	AA	15	37.60	1506.0	2.80	2.90	2.79	0.10	- 0.01
	NACL	15	37.60	1506.0	3.00	3.08	3.00	0.08	0.0
MEG-NACL	MEG	15	20.53	1600.6	20.0	20.0	19.97	0.0	- 0.03
	NACL	15	20.53	1600.6	3.0	2.70	3.02	- 0.3	0.02
MEG-NACL	MEG	15	27.70	1664.7	30.0	29.10	29.34	- 0.9	- 0.7
	NACL	15	27.70	1664.7	5.00	4.80	5.10	- 0.2	0.10

AA-NACL	AA	25	17.85	1509.9	1.50	1.60	1.45	0.10	- 0.05
	NACL	25	17.85	1509.9	1.00	1.24	0.99	0.24	- 0.01
AA-NACL	AA	25	47.51	1531.3	2.00	1.77	2.13	- 0.23	0.13
	NACL	25	47.51	1531.3	3.00	2.64	3.06	- 0.36	0.06
MEG-NACL	MEG	25	6.83	1634.4	30.0	30.0	30.0	0.0	0.0
	NACL	25	6.83	1634.4	1.00	0.99	1.34	- 0.01	0.34
MEG-NACL	MEG	25	26.31	1612.4	20.0	20.6	20.08	0.6	0.08
	NACL	25	26.31	1612.4	3.00	2.70	3.02	- 0.3	0.02

In Table 4.1, "EXP" represents the experimental data, "MM" stands for the results from the mathematical model, and "ANN" corresponds to the results from the artificial neural network model. "AD" denotes the absolute deviation, which is defined as the difference between the model-predicted concentrations and the experimental concentrations.

From the results, the artificial neural network model's predicted values ("ANN" in Table 4.1) exhibit better agreement with the experimental data ("EXP" in Table 4.1) compared to the predicted values from the mathematical model ("MM" in Table 4.1). Even in cases where both models have slightly larger deviations, such as in the solution containing 30.0 wt% MEG and 5.0 wt% NaCl, the deviation of -0.7 from the ANN is less than the -0.9 deviation from the MM. This larger deviation can be attributed to MEG inhibitor concentrations that fall beyond the range of the model training data.

5. CONCLUSION

A principal objective of this research was to provide analytical models capable of effectively interpreting and validating the C-V method. This endeavor utilized second-degree regression predictive models to formulate equations for electrical conductivity and velocity as functions of inhibitor and salt concentrations, alongside temperature. Subsequent model validation through MATLAB simulations consistently yielded results in alignment with the experimental dataset.

Furthermore, an Artificial Neural Network (ANN) model, an exemplar of artificial intelligence, was developed, harnessing extensive experimental data derived from various systems. This model, driven by conductivity, velocity, and temperature as input variables, excels in determining inhibitor and salt concentrations. Notably, the concentrations of inhibitors and salts derived from the ANN model exhibited closer concordance with experimental values.

With the agreement between the results of the ANN/MM models and the experimental values, the C-V experimental method can be interpreted with second-degree regression predictive models and new results predicted with ANN model. The accurate assessment of inhibitor concentrations by the models resulted to accurate prediction of phase boundary which is an instrumental facet in ascertaining the optimal dosage of hydrate inhibitors to be injected in flowlines to prevent hydrate formation.

REFERENCES

Argo, C. B., Blain, R. A., Osborne, C. G. & Priestley, I.D. (2012). Commercial deployment of low dosage hydrate inhibitors in a Southern North Sea 69 km wet-gas subsea pipeline. *SPE Production & Facilities*, 15, 130-134.

Avlonitis D., Danesh, A. & Todd A. C. (2014). Prediction of VL and VLL Equilibria of Mixtures Containing Petroleum Reservoir Fluids and Methanol with a Cubic EoS. *Fluid Phase Equilibra*, 94, 181-216.

Barker, J. W. & Gomez, R. K. (2000). Formation of Hydrate during Deep-water Drilling operation. *Journal of Petroleum Technologies*, 41(3), 297-301.

Bonyad, H., Zare, M., Mosayyebi, M. R., Mazloum, S. & Tohidi, B. (2021). Field Evaluation of A Hydrate Inhibition Monitoring System. *Offshore Mediterranean Conference*, Ravenna, Italy, 2011.

Carson, D. B. & Katz, D. L. (1942). *Natural Gas Hydrates*. Trans., AIME. 146, 150.

Clay, C. S. & Medwin H. (2017). *Acoustic Oceanography: Principles and Application*, New York, Wiley.

Fu, B., Neff, S., Mathur A. & Bakeev K. (2014). Application of low-dosage hydrate inhibitors in deepwater operations. *SPE Production and Facilities*, 17, 133-137.

Goodenough, T. I. J., Rajendram, V.S., Meyer, S. & Pretre, D. (2015). Detection and qualification of insoluble particles by ultrasound spectroscopy, *Ultrasonics*, 43, 231-235.

Hammerschmidt, E. G. (1934). Formation of Gas Hydrates in Natural-Gas Transmission Lines. *Industrial & Engineering Chemistry*, 26 (8), 851-*855.*

Henning, B., Daur, P.C., Prange, S., Dierks, K. & Hauptmann, P. (2017). *Ultrasonics*, 388, 799-803.

Jerie, K., Baranowski, A., Przybylski, J. & Glinski, J. (2004). Electrolytic solutions in ethylene glycol: ultrasonic and positron annihilation studies. *Physics Letters* A, 323, 148-153.

Katz, D. L. (1945). *Prediction of Conditions for Hydrate Formation in Natural Gases*. Trans., AIME 160, 140.

Lavallie, O., Ansari, A. A., O'Neil, S., Chazelas, O., Glenat, P. & Tohidi, B. (2022). Successful field application of an inhibitor concentration detection system in optimising the kinetic hydrate inhibitor (KHI) injection rates and reducing the risks associated with hydrate blockage. IPTC 13765, presented at the International Petroleum Technology Conference, Doha, Qatar.

Linga, P., Daraboina, N., Ripmeester, J. A. & Englezos, P. (2012). Enhanced rate of gas hydrate formation in a fixed bed column filled with sand compared to a stirred vessel. *Chemical Engineering Science*, 68 (1), 617-623.

Mohammadi, A. H. & Richon, D. (2016). Estimating the Hydrate Safety Margin in the Presence of Salt or Organic Inhibitor Using Refractive Index Data of Aqueous Solution. *Industrial Engineering Chem*istry *Research*, 45, 8207-8212.

Mohammadi, A. H., Martinez-Lopez, J. F. & Richon, D. (2007). Determination of hydrate stability zone using electrical conductivity data of salt aqueous solution. *Fluid Phase Equilibria*, 253, 36-41.

Ostergaard, K. K., Masoudi, R., Tohidi, B, Danesh, A. & Todd, A. C. (2015). General correlation for predicting the suppression of hydrate dissociation temperature in the presence of thermodynamic inhibitors. *Journal of Petroleum Science and Engineering*, 48(1–2), 70–80.

Sandengen, K. & Kaas, B. (2018). Estimation of Monoethylene glycol (MEG) content in water-MEG-NaCl+NaHCO3 solutions. *Journal of Chemical Engineering Data*, 51, 443-447.

Tohidi B., Chapoy A. & Yang J. (2009). *Developing a hydrate-monitoring system*. *SPE Projects, Facilities and Construction,* 4, 1-6.

Tohidi, B., Chapoy, A., Yang, J. F., Ahmadloo, F. & Valko, I. (2008). Hydrate Monitoring and Early Warning Systems. *Offshore Technology conference*.

Vibhu, I., Singh, A.K, Gupta M. & Shukla, J. P. (2004). Ultrasonic and IR investigation of N-H--N complexes in ternary mixtures. *Journal of Molecular Liquids*, 115, 1-3.

Vyas, J. C., Katti, V. R., Gupta, S. K. & Yakhmi, J.V. (2006). A non-invasive ultrasonic gas sensor for binary gas mixtures. *Sensors and Actuators B*, 115, 28-32.

Wilcox, W. I., Carson, D. B. & Katz, D. L. (1941). Natural Gas Hydrates, *Industrial Engineering Chemistry*, 33, 662.

Willmon, J. G. & Edwards, M. A. (2016). *From pre-commissioning to startup: Getting chemical injection right*. *SPE Production & Operations,* 21, 483-491.

Yan, J., Mazloum, S., Chapoy, A. & Tohid, B. (2014). Minimizing Hydrate Inhibitor Injection Rate. *International petroleum Technology conferenc*e.

Yang, J., Chapoy, A., Mazloum, S. & Tohidi, B. (2023). Development of a Hydrate Inhibition Monitoring System by Integration of Acoustic Velocity and Electrical Conductivity Measurements. *Journal of Exploration and Production: Oil and Gas Review*, 9 (1), 36-40.

Yousif, M. H. & Young, D. B. (1993). A Simple Correlation to Predict hydrate point Suppression in Drilling Fluid. *SPE/IADC Drilling conference*, Amsterdam.